

# A Dual Half-Bridge Converter With Hybrid Rectifier for DC Power Supply in Railway Systems

Lei Zhao , Member, IEEE, Zejia Luo , Zhun Fan , Senior Member, IEEE, and Yi Shi

**Abstract**—Dual half-bridge (DHB) converter is a recent innovation in the family of full-bridge converters, and it can achieve higher efficiency compared to the traditional converters. The DHB converters with center-tapped rectifier (CTR) and full-bridge rectifier (FBR) have been adopted in low (<100 V) and high (>200 V) output voltage applications, respectively. However, the output voltage is between 100 and 200 V in some applications, such as auxiliary railway dc power supply, both CTR and FBR can be the candidate and it is very indistinct to select the matched rectifier. To suit for such specific application, this article proposes a DHB converter with hybrid rectifier (Hyb-R). The Hyb-R is composed of a CTR section and an FBR section, which are connected in series by sharing two diodes. As a combined structure, the voltage stress of Hyb-R is between that of FBR and CTR, which makes Hyb-R well appropriate for dc power supply in railway systems. In this article, the operational principle and performance of the proposed converter are analyzed in depth. Three prototypes based on the DHB converters with CTR, FBR, and Hyb-R are built and tested, respectively. Experimental results show that the proposed converter can achieve a superior efficiency compared with other converters.

**Index Terms**—Dual half-bridge (DHB) converter, full-bridge converter, hybrid rectifier (Hyb-R), zero-voltage switching.

## I. INTRODUCTION

IN MODERN electric railway systems, the dc power supply is an important component, which supplies the interior lighting, battery charger, and control system [1]–[3]. The required voltage level is around 110 V, and the required power level is generally at least several kilowatt [3]–[6]. In addition, the galvanic isolation is required. The phase-shifted full-bridge (PSFB) converter is a preferred topology for dc power supply because of its simple structure and natural zero-voltage switching (ZVS) [7]. Generally, the primary structure of PSFB converter is fixed

while different rectifiers, such as full-bridge rectifier (FBR) and center-tapped rectifier (CTR), can be applied to suit for various applications in the secondary side of PSFB converter. The FBR has low transformer volt-ampere requirement and voltage stress but high conduction loss of diodes and it is widely adopted in high output voltage applications (>200 V), such as electric vehicle battery charger (250 ~ 400 V) [8] and plasma display panel power module (205 V) [9]. Compared to FBR, CTR can achieve lower conduction loss but higher voltage stress, and it is very popular in low output voltage applications (<100 V), such as server power system (12 V) [10] and charger for neighborhood EVs (36 ~ 72 V) [11]. However, for the dc power supply in railway systems, the output voltage is between 100 and 200 V, both CTR and FBR can be the candidate and it is very indistinct to select the matched rectifier.

On the other hand, the traditional PSFB converter has some serious problems, such as narrow ZVS range and large circulating current. Many auxiliary commutated full-bridge converters have been proposed to improve the performance of PSFB converter [12]–[16]. Generally, ZVS is achieved by using the energy stored in the inductive components to discharge the junction capacitance of switch. Therefore, the range of ZVS can be extended by introducing auxiliary inductors into full-bridge converter to increase the available ZVS energy. The introduced circuit is independent of load current and can guarantee ZVS capability from light load to heavy load. However, the auxiliary circuit brings additional conduction loss and more cost.

The PSFB converter with zero-voltage and zero-current switching operation can provide effective solution to the problems [17]–[20]. In these converters, the leading-leg switches are turned ON with ZVS and the lagging-leg switches are turned OFF with ZCS. The ZVS operation is obtained in the same way as that of the conventional PSFB converter and the ZCS operation is created by introducing an auxiliary voltage source to reset the primary current. However, the primary power cannot be transferred to the output side during the freewheeling interval and large filter requirement is needed in wide-input-voltage-range applications.

Dual half-bridge (DHB) converter is another effective solution to improve the performance of full-bridge converter [21]–[26]. Compared to the traditional PSFB converter, the DHB converter has the following advantages.

- 1) The available ZVS energy is enough to achieve a wide ZVS range.
- 2) The circulating current is removed, which contributes to the reduction of conduction loss.

Manuscript received December 16, 2018; revised April 6, 2019, June 1, 2019, and August 4, 2019; accepted September 22, 2019. Date of publication October 6, 2019; date of current version February 11, 2020. This work was supported in part by STU Scientific Research Foundation for Talents under Grant NTF18008, in part by the National Natural Science Foundation of China under Grants 61801283 and 51907113, and in part by the Foundation for Distinguished Young Talents in Higher Education of Guangdong under Grant 2018KQNCX080. Recommended for publication by Associate Editor N. R. Zargari. (Corresponding author: Zhun Fan).

The authors are with the Department of Electronic and Information Engineering and the Guangdong Provincial Key Laboratory of Digital Signal and Image Processing, Shantou University, Shantou 515063, China, and also with the Key Laboratory of Intelligent Manufacturing Technology (Shantou University), Ministry of Education, Shantou 515063, China (e-mail: zhaoleichinese@163.com; 18zjluo@stu.edu.cn; zfan@stu.edu.cn; shy\_xflx@163.com).

Color versions of one or more of the figures in this article are available online at <http://ieeexplore.ieee.org>.

Digital Object Identifier 10.1109/TPEL.2019.2946046

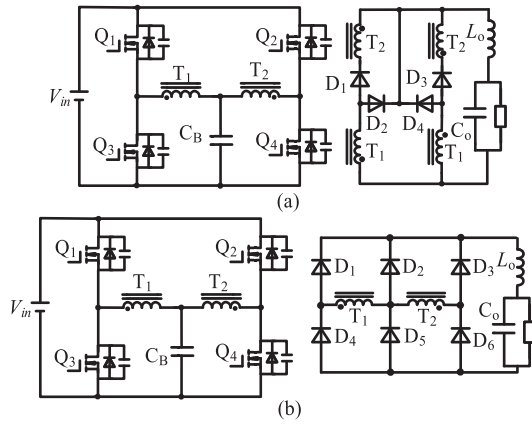


Fig. 1. DHB converters with different rectifiers. (a) CTR. (b) FBR.

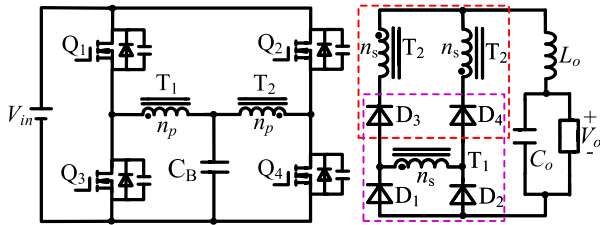


Fig. 2. Proposed DHB converters with Hyb-R.

- 3) The primary power can be continually transferred to the secondary side and the output filter requirement is significantly reduced.

The primary side of DHB converter is composed of a lagging half-bridge inverter and a leading half-bridge inverter, which are placed in parallel with input voltage. Various rectified structures can be adopted in the secondary side. Fig. 1 shows the DHB converters with FBR [21] and CTR [22]. Compared to CTR, FBR presents advantage in terms of voltage stress of diodes although six diodes are adopted. On the other hand, only four diodes are adopted in CTR and only one diode conducts during the power transmission, resulting in less conduction loss. The converters with FBR are widely employed in high voltage applications, whereas the converters with CTR are widely employed in low voltage applications.

Based on the DHB converters with FBR and CTR, a novel DHB converter with hybrid rectifier (Hyb-R) is proposed in this article, as shown in Fig. 2. The Hyb-R is composed of a FBR section and a CTR section, which are connected in series by sharing two rectified diodes. The total number of diodes and secondary windings in Hyb-R is the least compared with FBR and CTR. As a combined structure of FBR and CTR, the maximum voltage stress, switching loss, and conduction loss of Hyb-R diodes are between CTR and FBR. These features make the proposed converter well appropriate for the medium output voltage applications.

The detailed operational principle of the proposed converter is analyzed in Section II. Section III then analyzes the performance of the converter. A 1.2-kW hardware prototype with 380–450 V

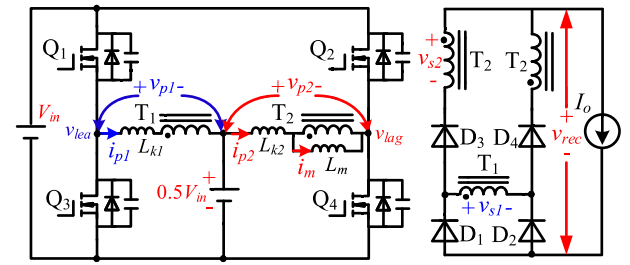


Fig. 3. Equivalent circuit with current and voltage notations.

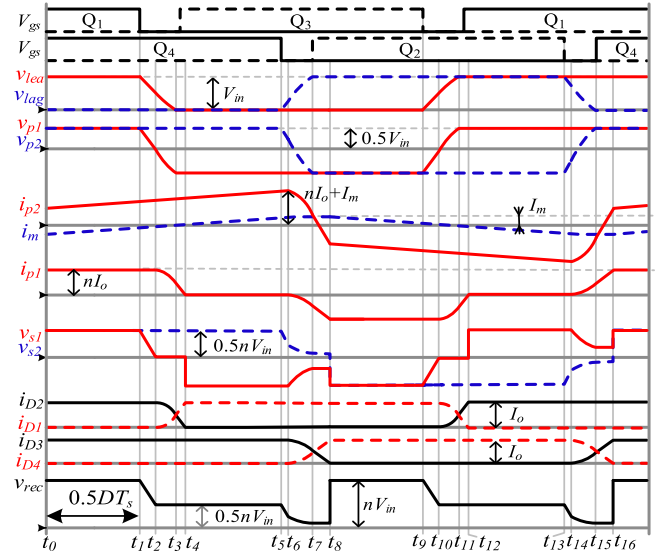


Fig. 4. Key waveforms of the proposed converter.

input 120 V/10 A output is built and tested to verify the theory analysis in Section IV. In addition, two prototypes based on the DHB converters with FBR and CTR are also built to compare with the proposed Hyb-R converter. Section V concludes this article.

## II. OPERATIONAL PRINCIPLE

Fig. 3 shows the equivalent circuit with current and voltage notations. To simplify analysis, the following assumptions are made:

- 1) the output filter inductor  $L_o$  is modeled as a constant current source;
- 2) the output capacitor  $C_o$  and the blocking capacitor  $C_B$  are considered as constant voltage sources of  $V_o$  and  $0.5V_{in}$ , respectively;
- 3) the leakage inductances of  $T_1$  and  $T_2$  are  $L_{k1}$  and  $L_{k2}$ , respectively. The magnetizing inductance of  $T_2$  is  $L_m$  and the magnetizing inductance of  $T_1$  is large enough to ignore the effect;
- 4) the junction capacitances of MOSFETs are  $C_{oss}$ ;
- 5)  $T_1$  and  $T_2$  have the same turns ratio of  $n = n_s/n_p$ .

Fig. 4 shows the key waveforms of the proposed converter, where  $T_s$  is switching period and  $D$  means duty cycle of rectified voltage. In order to show the detailed waveforms during the ZVS

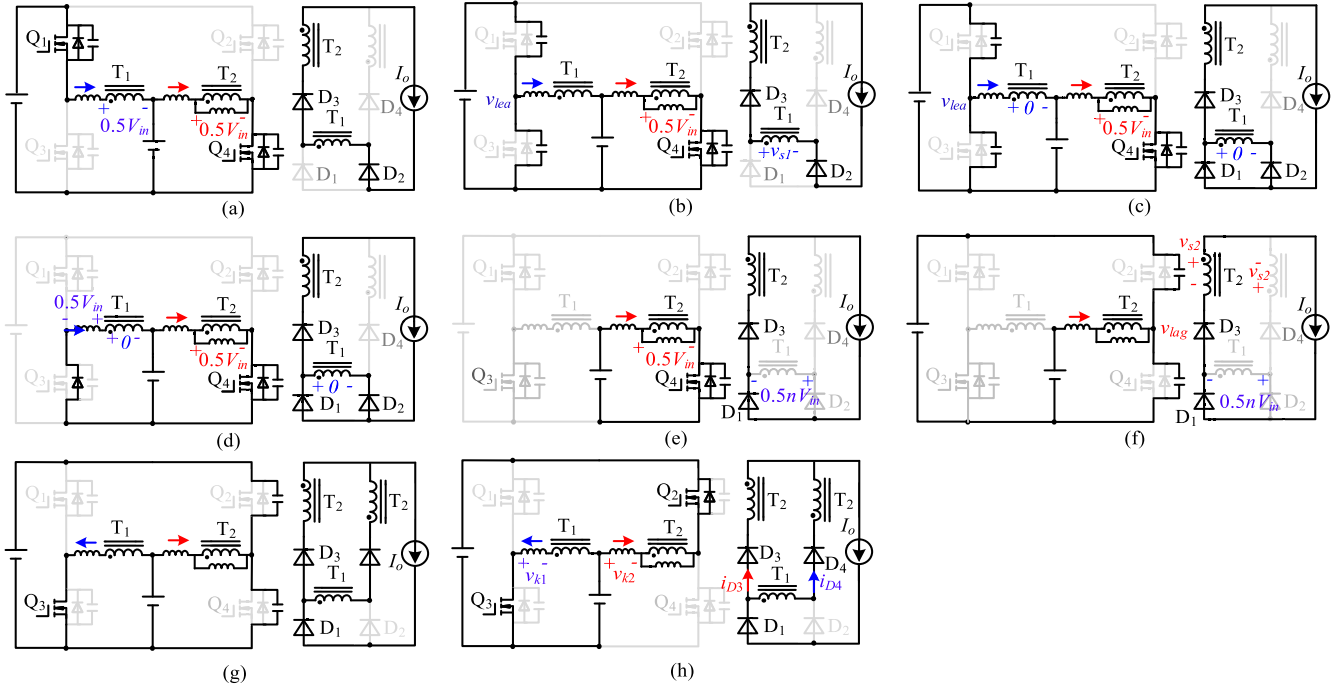


Fig. 5. Equivalent circuits in the first half cycle. (a) State 1 [ $t_0 \sim t_1$ ]. (b) State 2 [ $t_1 \sim t_2$ ]. (c) State 3 [ $t_2 \sim t_3$ ]. (d) State 4 [ $t_3 \sim t_4$ ]. (e) State 5 [ $t_4 \sim t_5$ ]. (f) State 6 [ $t_5 \sim t_6$ ]. (g) State 7 [ $t_6 \sim t_7$ ]. (h) State 8 [ $t_7 \sim t_8$ ].

transition, the transition times are enlarged in Fig. 4. The phase-shifted control method is employed.  $Q_1$ - $Q_3$  form the leading-leg and  $Q_2$ - $Q_4$  form the lagging-leg. The output voltage is regulated by adjusting the phase time  $0.5DT_s$  between the leading-leg and the lagging-leg. There are 16 states in one switching period, which can be divided into two half cycles,  $t_0 \sim t_8$  and  $t_8 \sim t_{16}$ . Due to the symmetry of the circuit, only the first half cycle is analyzed here and the corresponding equivalent circuits are shown in Fig. 5.

**State 1 [ $t_0 \sim t_1$ ]:** In this state,  $Q_1$  and  $Q_4$  are ON and  $D_2$  and  $D_3$  are conducting. The primary voltages of  $T_1$  and  $T_2$  are  $0.5V_{in}$  and the rectified voltage  $v_{rec}(t)$  is equal to the sum of secondary voltages of  $T_1$  and  $T_2$ , i.e.,  $nV_{in}$ . This state is defined as duty-cycle interval. During this interval, both lagging-leg and leading-leg can transfer the primary energy to the output side. The leading-leg current is maintained at  $nI_o$  and the magnetizing current  $i_m(t)$  increases linearly from its minimum value. The primary currents can be calculated as follows:

$$i_m(t) = -I_m + \frac{0.5V_{in}}{L_m}(t - t_0) \quad (1)$$

$$i_{p2}(t) = nI_o + i_m(t). \quad (2)$$

**State 2 [ $t_1 \sim t_2$ ]:** At  $t_1$ ,  $Q_1$  is turned OFF with ZVS due to the existence of junction capacitances. The duration time of this state is very short, and all the primary currents are considered as constants. The leading-leg current  $i_{p1}$  starts to charge/discharge the junction capacitance of  $Q_1/Q_3$ . The leading-leg voltage  $v_{lea}(t)$  and the secondary voltage  $v_{s1}(t)$

of  $T_1$  linearly decrease

$$v_{lea}(t) = V_{in} - \frac{nI_o}{2C_{oss}}(t - t_1) \quad (3)$$

$$v_{s1}(t) = n[v_{lea}(t) - 0.5V_{in}]. \quad (4)$$

**State 3 [ $t_2 \sim t_3$ ]:** At  $t_2$ ,  $v_{lea}(t)$  falls to  $0.5V_{in}$  and  $v_{s1}(t)$  falls to zero.  $D_1$  starts to conduct and the secondary voltage of  $T_1$  is clamped to zero by  $D_1$  and  $D_2$ . At the same time, the resonance of  $L_{k1}$  and  $2C_{oss}$  occurs in the leading-leg. According to the initial conditions and Kirchoff's law, the voltage and current of leading-leg can be expressed as

$$i_{p1}(t) = nI_o \cos\omega_1(t - t_2) \quad (5)$$

$$v_{lea}(t) = 0.5V_{in} - nI_o L_{k1} \omega_1 \sin\omega_1(t - t_2) \quad (6)$$

where  $\omega_1 = 1/\sqrt{2C_{oss}L_{k1}}$ .

**State 4 [ $t_3 \sim t_4$ ]:** At  $t_3$ ,  $v_{lea}(t)$  falls to zero. Then, the parasitic diode of  $Q_3$  begins to conduct and  $Q_3$  can be turned ON with ZVS. During this state,  $v_{s1}$  is maintained at zero and the voltage  $0.5V_{in}$  appears on  $L_{k1}$ . Due to this voltage across  $L_{k1}$ , the leading-leg current linearly decreases. The commutation between  $D_1$  and  $D_2$  is progressed,  $i_{D1}(t)$  increases and  $i_{D2}(t)$  decreases. This state ends when  $i_{D2}(t)$  falls to zero at  $t_4$ .

**State 5 [ $t_4 \sim t_5$ ]:** At  $t_4$ , the commutation between  $D_1$  and  $D_2$  is completed,  $D_2$  turns OFF naturally and the leading-leg current falls to zero. The primary voltage of  $T_2$   $v_{p2}(t)$  is  $0.5V_{in}$  and the rectified voltage is equal to the secondary voltage of  $T_2$ , i.e.,  $0.5nV_{in}$ . This state is defined as freewheeling interval. During this state, the primary power is transferred to the secondary side through only the lagging-leg.

*State 6* [ $t_5 \sim t_6$ ]: At  $t_5$ ,  $Q_4$  is turned OFF and the magnetizing current  $i_m(t)$  reaches to the maximum value  $I_m$ . During this state, the lagging-leg current can be considered as a constant current source of  $nI_o + I_m$ . The junction capacitances of lagging-leg switches are linearly charged by this current source. The key voltages in this state can be calculated as follows:

$$v_{\text{lag}}(t) = \frac{nI_o + I_m}{2C_{\text{oss}}}(t - t_5) \quad (7)$$

$$v_{s2}(t) = v_{\text{rec}}(t) = n[0.5V_{\text{in}} - v_{\text{lag}}(t)] \quad (8)$$

$$v_{s1}(t) = -0.5nV_{\text{in}}. \quad (9)$$

The voltage across  $D_4$  is

$$v_{D4}(t) = 2v_{s2}(t) + v_{s1}(t). \quad (10)$$

Based on the equations,  $v_{D4}$  decreases linearly. At  $t_6$ ,  $v_{D4}(t)$  falls to zero and  $D_4$  starts to conduct. Therefore,  $v_{s2}(t_6)$  is  $0.25nV_{\text{in}}$  and  $v_{\text{lag}}(t_6)$  is  $0.25V_{\text{in}}$ .

*State 7* [ $t_6 \sim t_7$ ]: During this state, the commutation between  $D_3$  and  $D_4$  is progressed and the resonance of junction capacitances and leakage inductances occurs in the primary side. The lagging-leg voltage  $v_{\text{lag}}(t)$  increases and the voltage across  $Q_2$  decreases with sinusoidal shapes, respectively. Based on the equivalent circuit and the initial conditions at  $t_6$ , the key currents and voltages in this state are given by

$$i_{p2}(t) = (nI_o + I_m)\cos\omega_2(t - t_6) \quad (11)$$

$$i_{p1}(t) = -0.5(nI_o + I_m)[1 - \cos\omega_2(t - t_6)] \quad (12)$$

$$v_{\text{lag}}(t) = 0.25V_{\text{in}} + (nI_o + I_m)(0.25L_{k1} + L_{k2})\omega_2\sin\omega_2(t - t_6) \quad (13)$$

$$v_{Q2}(t) = V_{\text{in}} - v_{\text{lag}}(t) \quad (14)$$

where  $\omega_2 = 1/\sqrt{2C_{\text{oss}}(0.25L_{k1} + L_{k2})}$ .

*State 8* [ $t_7 \sim t_8$ ]: At  $t_7$ , the voltage across  $Q_2$  falls to zero and  $Q_2$  can be turned ON with ZVS. During this state, the voltages of leakage inductors can be expressed as follows:

$$v_{k1}(t) = -\frac{0.375L_{k1}}{L_{k2} + 0.25L_{k1}}V_{\text{in}} \quad (15)$$

$$v_{k2}(t) = -\frac{0.75L_{k2}}{L_{k2} + 0.25L_{k1}}V_{\text{in}}. \quad (16)$$

Due to the existence of  $v_{k1}(t)$  and  $v_{k2}(t)$ , the currents of leading-leg and lagging-leg rise in the negative direction. In the secondary side, the commutation between  $D_3$  and  $D_4$  is continually progressed,  $i_{D3}(t)$  decreases and  $i_{D4}(t)$  increases linearly. The key currents are expressed as follows:

$$i_{p2}(t) = i_{p2}(t_7) + \frac{v_{k2}(t)}{L_{k2}}(t - t_7) \quad (17)$$

$$i_{p1}(t) = i_{p1}(t_7) + \frac{v_{k1}(t)}{L_{k1}}(t - t_7) \quad (18)$$

$$i_{D4}(t) = -\frac{i_{p1}(t)}{n} \quad (19)$$

$$i_{D3}(t) = I_o - i_{D4}(t). \quad (20)$$

At the end of this state,  $i_{D4}(t)$  reaches to  $I_o$ ,  $i_{D3}(t)$  falls to zero, and  $D_3$  is naturally turned OFF. Then,  $T_1$  and  $T_2$  simultaneously transfer the input power to the secondary side.

### III. PERFORMANCE ANALYSIS AND COMPARISON

#### A. Voltage Conversion Ratio

Since the durations of ZVS transitions are very narrow, only *State 1* and *State 5* are considered. The rectified voltage during the duty-cycle interval (*State 1*) is  $nV_{\text{in}}$ , whereas it is  $0.5nV_{\text{in}}$  during the freewheeling interval (*State 5*). The output voltage is equal to the average of rectified voltage. Therefore, the voltage conversion ratio is given by

$$G(D) = V_o/nV_{\text{in}} = 0.5(1 + D). \quad (21)$$

#### B. ZVS Condition

Based on the operational principle of proposed converter, the ZVS transition of leading-leg switches can be divided into two phases, *State 2* [ $t_1 \sim t_2$ ] and *State 3* [ $t_2 \sim t_3$ ]. In the first phase, the output filter inductor participates in ZVS transition and the leading-leg voltage  $v_{\text{lea}}(t)$  decreases linearly, as shown in Fig. 5(b). When  $v_{\text{lea}}(t)$  falls to  $0.5V_{\text{in}}$  at  $t_2$ , the resonance between leakage inductance  $L_{k1}$  and junction capacitance  $2C_{\text{oss}}$  occurs in the leading-leg and  $v_{\text{lea}}(t)$  decreases with a sinusoidal waveform, as shown in Fig. 5(c). The leading-leg switches can achieve ZVS at the end of the secondary phase. The ZVS condition of leading-leg switches is obtained from (6) as follow:

$$nI_oL_{k1}\omega_1 > 0.5V_{\text{in}}. \quad (22)$$

In the view of energy, (22) can be rewritten as

$$\frac{1}{2}L_{k1}(nI_o)^2 > \frac{4}{3}C_{\text{oss}}(0.5V_{\text{in}})^2. \quad (23)$$

It can be noted from (23) that the remaining energy in the junction capacitors, which should be discharged by the leakage inductor  $L_{k1}$ , is one quarter of the total energy.

The ZVS transition of lagging-leg switches is also divided into two phases, *State 6* [ $t_5 \sim t_6$ ] and *State 7* [ $t_6 \sim t_7$ ]. The lagging-leg voltage linearly increases from 0 to  $0.25V_{\text{in}}$  at first and then increases with a sinusoidal waveform due to the resonance of leakage inductances and junction capacitances. The ZVS condition of lagging-leg switches is obtained from (13) as

$$(nI_o + I_m)(0.25L_{k1} + L_{k2})\omega_2 > 0.75V_{\text{in}}. \quad (24)$$

In the view of energy, (24) can be rewritten as

$$\frac{1}{2}(0.25L_{k1} + L_{k2})(nI_o + I_m)^2 > \frac{4}{3}C_{\text{oss}}(0.75V_{\text{in}})^2. \quad (25)$$

According to (25), the magnetizing current  $I_m$  contributes to the ZVS and the ZVS range can be extended by increasing  $I_m$ . However, large magnetizing current increases the conduction losses of primary switches and transformers. Fig. 6(a) shows

TABLE I  
 COMPARISON OF DHB CONVERTER WITH DIFFERENT RECTIFIERS

Rectifier	CTR	Hyb-R	FBR
Number of secondary winding	4	3	2
Number of diode	4	4	6
Voltage conversion ratio	$0.5(1+D)$	$0.5(1+D)$	$0.5(1+D)$
ZVS condition of leading-leg	$\frac{1}{2}L_{k1}(nI_o)^2 > \frac{4}{3}C_{oss}(0.5V_{in})^2$	$\frac{1}{2}L_{k1}(nI_o)^2 > \frac{4}{3}C_{oss}(0.5V_{in})^2$	$\frac{1}{2}L_{k1}(nI_o)^2 > \frac{4}{3}C_{oss}(0.5V_{in})^2$
ZVS condition of lagging-leg	$\frac{1}{2}(0.25L_{k1} + L_{k2})(nI_o + I_m)^2 > \frac{4}{3}C_{oss}(0.75V_{in})^2$	$\frac{1}{2}(0.25L_{k1} + L_{k2})(nI_o + I_m)^2 > \frac{4}{3}C_{oss}(0.75V_{in})^2$	$\frac{1}{2}(L_{k1} + L_{k2})(nI_o + I_m)^2 > \frac{4}{3}C_{oss}V_{in}^2$
Voltage stress of diode	$D_1, D_3 : 2nV_{in}$ $D_2, D_4 : 1.5nV_{in}$	$D_3, D_4 : 1.5nV_{in}$ $D_1, D_2 : 0.5nV_{in}$	$D_1, D_3, D_4, D_6 : nV_{in}$ $D_2, D_5 : 0.5nV_{in}$
Power loss	High switching loss Low conduction loss	Medium switching loss Medium conduction loss	Low switching loss High conduction loss

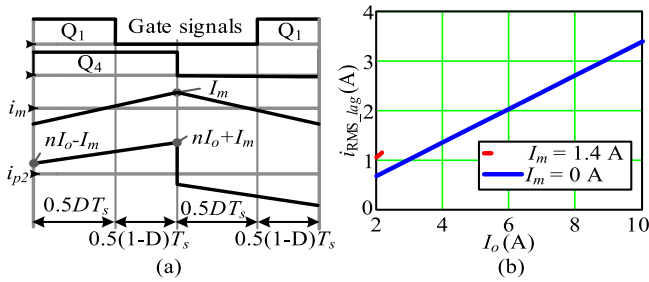


Fig. 6. (a) Simplified waveform of lagging-leg current. (b) RMS current of lagging-leg versus load current.

the simplified waveform of lagging-leg current. The rms current of lagging-leg is approximately evaluated as

$$i_{\text{RMS\_lag}} = nI_o \sqrt{1 + \frac{1}{3} \left( \frac{I_m}{nI_o} \right)^2}. \quad (26)$$

Fig. 6(b) shows the rms current versus load current. Since the average value of magnetizing current is zero during a half switching period, its contribution to the total rms current can be negligible, as shown in Fig. 6(b). Therefore, large magnetizing current has a little impact on the conduction loss but it is benefit to extend the ZVS range of lagging-leg switches.

### C. Performance Comparison

In this section, the DHB converters with CTR and FBR are selected to compare with the proposed converter. The structure of rectifier, voltage conversion ratio, ZVS conditions, voltage stress of diodes, and power loss of different rectifiers are considered for comparison, as shown in Table I.

1) *Structure of rectifier*: The CTR contains four secondary windings and four rectified diodes, and only one diode conducts during the power transmission. On the other hand, the FBR requires two secondary windings and six diodes, and two diodes simultaneously conduct. The Hyb-R is consisted of three secondary windings and four

diodes. Therefore, the total number of secondary windings and diodes in the proposed Hyb-R is the least.

- 2) *Voltage conversion ratio*: The rectified voltage is  $nV_{in}$  during the duty-cycle interval and it is  $0.5nV_{in}$  during the freewheeling interval. Therefore, the DHB converters with different rectifiers have the same voltage conversion ratio. Moreover, since the output filter inductor is designed based on the rectified voltage, they also have the same filter requirement.
- 3) *ZVS conditions*: The DHB converters with CTR and Hyb-R have the same ZVS conditions, and the required energy for lagging-leg ZVS transition in them is smaller than that in the DHB converter with FBR. The magnetizing currents in these converters can be used to extend the ZVS range of lagging-leg switches without causing extra conduction losses and high current stress. Compared to the traditional PSFB converter, all of the DHB converters can achieve a wide ZVS range with small leakage inductances.
- 4) *Voltage stress of rectified diodes*: In order to simplify analysis, the secondary voltage oscillation caused by parasitic circuit elements is ignored. Fig. 7 shows the equivalent circuits of rectifier stages in different DHB converters. The voltage stress of diodes can be calculated based on Fig. 7. The maximum voltage stress in CTR, Hyb-R, and FBR are  $2nV_{in}$ ,  $1.5nV_{in}$ , and  $nV_{in}$ , respectively. CTR diodes withstand the highest voltage stress and FBR diodes withstand the lowest voltage stress. Therefore, CTR is suited for low output voltage applications and FBR is suited for high output voltage applications. As a combined structure of FBR and CTR, the maximum voltage stress of Hyb-R diodes is in the middle of CTR and FBR. Hence, the proposed Hyb-R is suited for medium voltage applications. In addition, the voltage stress of  $D_1$  and  $D_2$  in Hyb-R are very low and they can use low-voltage rating diodes, such as Schottky diode. Therefore, the conduction losses of diodes can be considerably reduced.
- 5) *Power loss of rectifiers*: The loss of rectifier generally contains conduction loss and switching loss, and they can be calculated approximately using the datasheet values [27], [28]. The conduction loss is caused by the forward

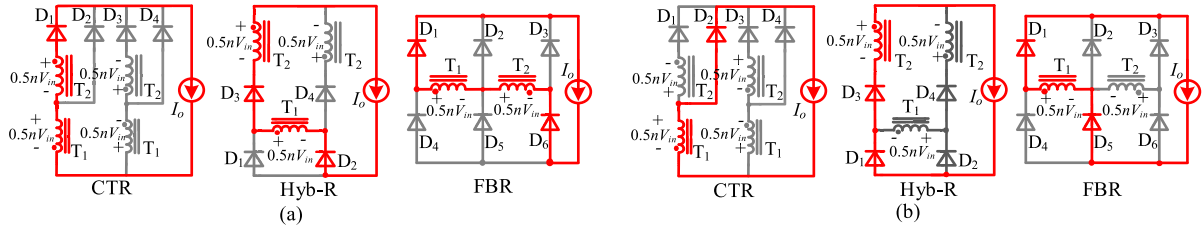


Fig. 7. Equivalent circuits of rectifier stages during (a) Duty-cycle interval. (b) Freewheeling interval.

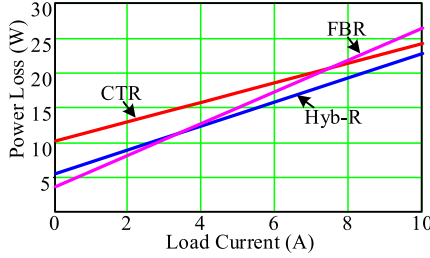


Fig. 8. Total loss of different rectifiers.

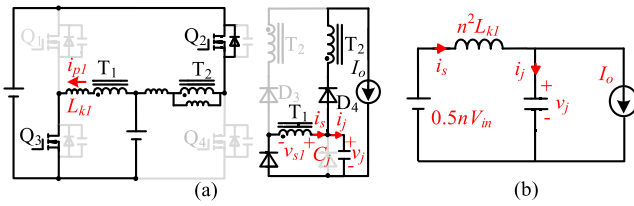


Fig. 9. Equivalent circuit during  $[t_8\sim]$ . (a) Detailed equivalent circuit. (b) Simplified equivalent circuit.

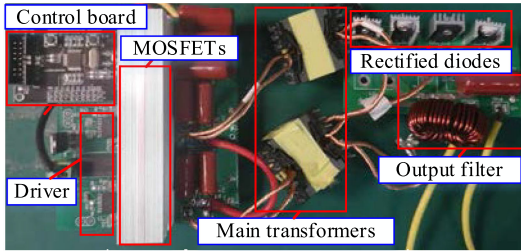


Fig. 10. Photograph of the proposed converter.

TABLE II  
PARAMETERS OF THE PROPOSED PROTOTYPE

Item	Symbol	Value/Part
Input Voltage	$V_{in}$	380~450 V
Output Voltage	$V_o$	120 V
Output Current	$I_o$	10 A
Switching Frequency	$f_s$	100 kHz
Blocking Capacitor	$C_B$	4.7 $\mu$ F
Output Inductor	$L_o$	130 $\mu$ H
Output Capacitor	$C_o$	80 $\mu$ F
Primary Switches	$Q_1 \sim Q_4$	SPW20N60C3
Rectified Diodes	$D_1, D_2$	12TQ150
	$D_3, D_4$	DPG151400PM
Main transformers ( $T_1, T_2$ )		Core: PQ3535, $n = 0.34$ For $T_1$ : $L_k = 5 \mu$ H, $L_m = 1$ mH; For $T_2$ : $L_k = 6.8 \mu$ H, $L_m = 0.4$ mH.

TABLE III  
SPECIFICATIONS OF RECTIFIED DIODES

	Part number	$V_{RPM}$	$V_F$
CTR	$D_1, D_3$ : DSEP15-06A	600 V	1.35 V
	$D_2, D_4$ : DPG151400PM	400 V	1.14 V
Hyb-R	$D_3, D_4$ : DPG151400PM	400 V	1.14 V
	$D_1, D_2$ : 12TQ150	150 V	0.63 V
FBR	$D_1, D_3, D_4, D_6$ : DPG151300PA	300 V	1.01 V
	$D_2, D_5$ : 12TQ150	150 V	0.63 V

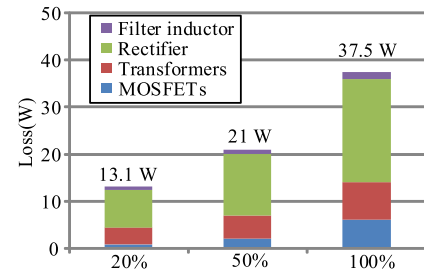


Fig. 11. Loss breakdown at different load currents.

voltage drop of diode and it is the main contributor to the total diode power loss under heavy load conditions. Therefore, the use of diode with low forward voltage drop, such as Schottky diode, can considerably reduce the conduction loss and improve the conversion efficiency. However, the peak reverse voltage of Schottky diode is limited to 200 V and it is widely adopted only in low output voltage applications. The switching loss is mainly decided by the reverse voltage, reverse current, and reverse recovery time of diode and it makes up almost all of the diode power loss at light loads. Fig. 8 shows the total loss of different rectifiers versus load current. As shown in Fig. 8, the loss of FBR is the smallest at light loads due to low switching loss, whereas it is the highest at heavy loads due to high conduction loss. The total loss of CTR is contrary to that of FBR because of high switching loss and low conduction loss. As a combined structure of FBR and CTR, both the switching loss and conduction loss of Hyb-R are between CTR and FBR, and the total loss is the least under medium and heavy load conditions.

#### D. Analysis of Ringing Mechanism

The ringing voltage and current are caused by the resonance between leakage inductance of transformer and junction capacitance  $C_j$  of rectified diode after the lagging-leg transition

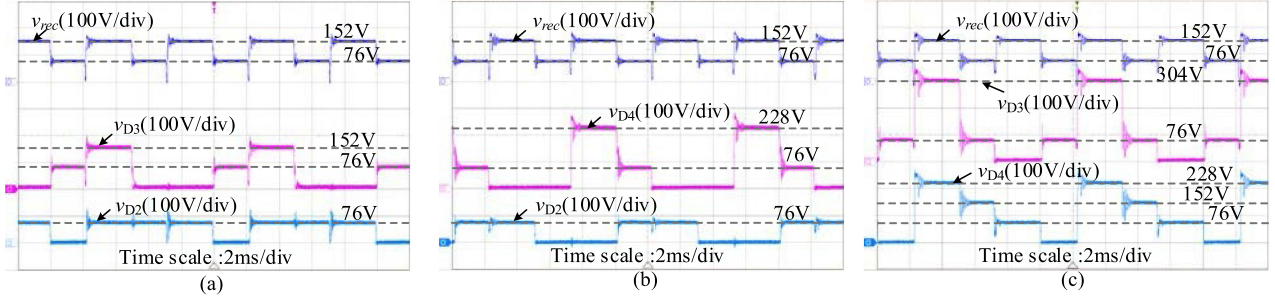


Fig. 12. Key waveforms of secondary voltages at  $V_{in} = 450$  V and  $I_o = 10$  A in the (a) FBR converter, (b) Hyb-R converter, and (c) CTR converter.

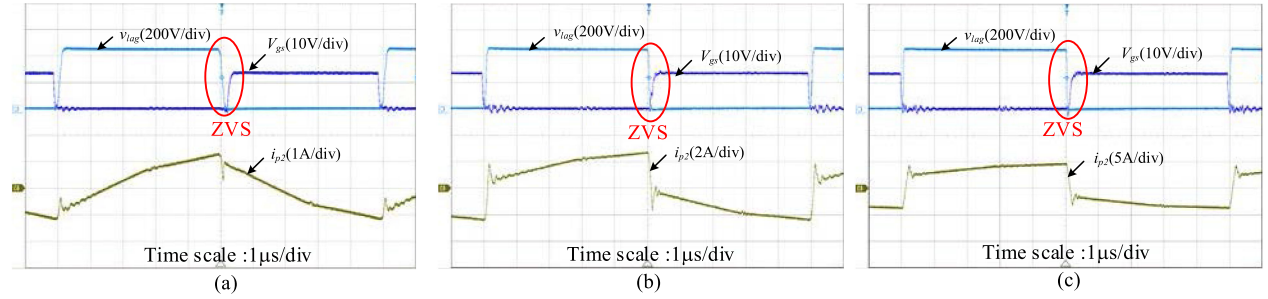


Fig. 13. ZVS waveforms of lagging-leg switch at  $V_{in} = 450$  V. (a) 1 A. (b) 5 A. (c) 10 A.

[29], [30]. The junction capacitance of diode is ignored to simplify the analysis when the operation principle is introduced in Section II. In the experimental prototype,  $D_1$  and  $D_2$  are selected as 12TQ150 ( $C_j \approx 100$  pF) [31], whereas  $D_3$  and  $D_4$  are selected as DPG151400PM ( $C_j \approx 16$  pF) [32]. In this part, only the junction capacitances of  $D_1$  and  $D_2$  are considered to analyze the ringing mechanism. After the lagging-leg transition is finished at  $t_8$ , the leakage inductances and junction capacitances constitute the resonant circuit, as shown in Fig. 9.

Based on Fig. 9(b), the ringing voltage and current are expressed as

$$v_j(t) = 0.5nV_{in} + (v_{j0} - 0.5nV_{in})\cos\omega_j t \quad (27)$$

$$i_{p1}(t) = nI_o - n(v_{j0} - 0.5nV_{in})C_j\omega_j\sin\omega_j t \quad (28)$$

where  $\omega_j = 1/n\sqrt{C_j L_{k1}}$ , and  $v_{j0}$  means the initial voltage of  $C_j$ .

#### IV. EXPERIMENTAL RESULTS

To verify the theoretical analysis, a laboratory prototype based on the proposed converter was built, as shown in Fig. 10. The parameters of the prototype are described in Table II. In order to compare the performance of the proposed converter with other DHB converters, two prototypes based on FBR and CTR are also built. The biggest difference between the three prototypes is the parameters of rectified diodes. The specifications of diodes in three prototypes are listed in Table III.  $V_F$  means forward voltage drop and  $V_{RPM}$  means repetitive peak reverse voltage. Fig. 11 shows the loss breakdown of the proposed converter under different load conditions. It can be seen that the loss

of rectifier makes up more than half of the total power loss. Therefore, the structure of rectifier has a significant effect on the overall power conversion efficiency.

Fig. 12 shows the experimental waveforms of rectified voltages and voltages across diodes in the DHB converters with FBR, Hyb-R, and CTR, respectively. As shown in Fig. 12, the rectified voltage during the duty-cycle interval is almost double that during the freewheeling interval in all the converters. Therefore, the converters with different rectifiers have the same voltage conversion gain. If the secondary voltage oscillation is ignored, the maximum voltage stresses of diodes in FBR, Hyb-R, and CTR are  $nV_{in}$ ,  $1.5nV_{in}$ , and  $2nV_{in}$ , respectively. CTR diodes withstand the highest voltage stress and it is suited for low output voltage applications. On the other hand, FBR diodes withstand the lowest voltage stress and it is suited for high output voltage. As a combined structure of FBR and CTR, the maximum voltage stress of Hyb-R diodes is in the middle of CTR and FBR. Hence, Hyb-R is suited for medium output voltage applications. The experimental results coincide well with the theoretical analysis.

Figs. 13 and 14 show the ZVS waveforms of lagging-leg and leading-leg switches at different load currents, respectively. It can be seen that all the switches are turned-ON after the drain-source voltages drop to zero. Therefore, the proposed converter can achieve a wide ZVS range.

Fig. 15 shows the key experimental waveforms of the DHB converter with Hyb-R at  $V_{in} = 450$  V and  $I_o = 10$  A. It can be noted that the durations of ZVS transitions are very narrow in fact. As shown in Fig. 15(a), the leading-leg current  $i_{p1}$  falls to zero after the ZVS transition starts. Therefore, the power flowing through the leading-leg is zero during the freewheeling interval.

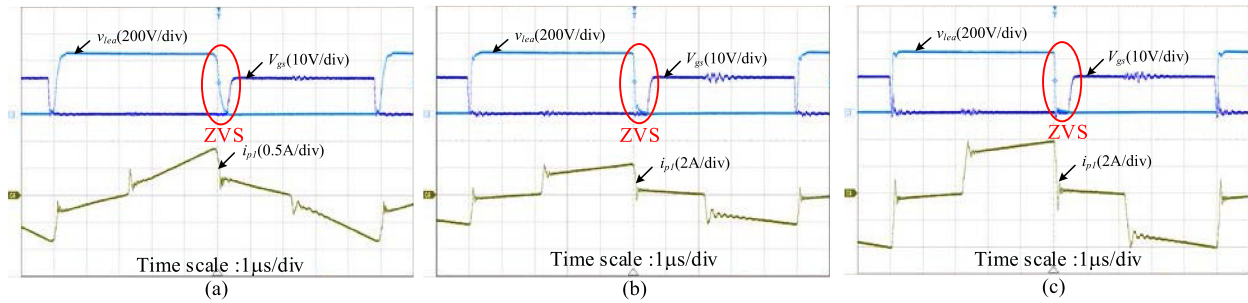


Fig. 14. ZVS waveforms of leading-leg switch at  $V_{in} = 450$  V. (a) 1 A. (b) 5 A. (c) 10 A.

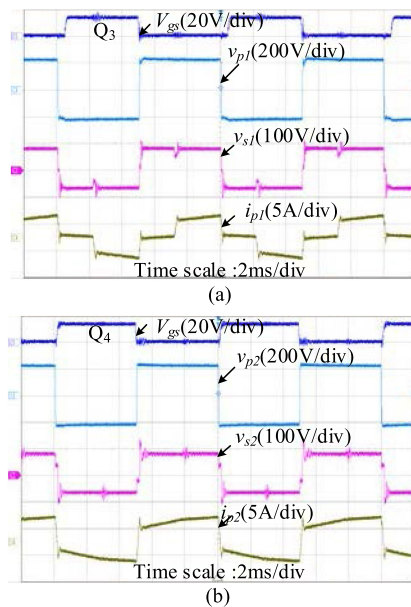


Fig. 15. Experimental waveforms at  $V_{in} = 450$  V and  $I_o = 10$  A. (a) Leading-leg. (b) Lagging-leg.

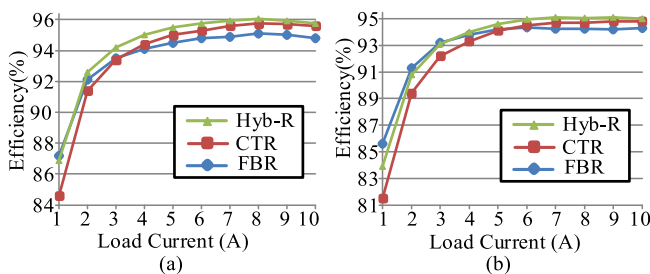


Fig. 16. Measured efficiency at (a)  $V_{in} = 380$  V and (b)  $V_{in} = 450$  V.

On the other hand, the lagging-leg current  $i_{p2}$  are nonzero during the whole switching period, as shown in Fig. 15(b). The lagging-leg can continually transfer the primary power to the secondary side.

The impact of different rectifiers on the efficiency of the prototypes is depicted in Fig. 16. As shown in Fig. 16, the efficiency of FBR prototype is higher than that of CTR prototype at  $I_o = 1$  A due to low switching loss, whereas it is lower than the

efficiency of CTR prototype at heavy load due to high conduction loss. As a combined structure, the proposed Hyb-R prototype can achieve an improved efficiency over wide ranges of load current and input voltage since the switching loss and the conduction loss of Hyb-R are between that of FBR and CTR. It should be noted that the efficiency improvement is very limited under heavy load conditions compared to the CTR prototype. This is due to that the conduction loss is the main contributor to the total power loss and the forward voltage drop of CTR is the smallest among the three rectifiers.

## V. CONCLUSION

This article proposes a novel DHB converter with Hyb-R. The Hyb-R is composed of a FBR section and a CTR section, which are connected in series by sharing two rectified diodes. The total number of rectified diodes and secondary windings in Hyb-R is the least compared with FBR and CTR. As a combined structure of FBR and CTR, the maximum voltage stress of Hyb-R is between that of FBR and CTR, which makes it well suited for the dc power supply in railway systems. Compared to the CTR converter, the Hyb-R converter can adopt low-voltage rating rectified diodes. This feature is beneficial for decreasing the conduction loss and switching loss. Compared to the FBR converter, the proposed converter requires fewer number of rectified diodes and achieves higher efficiency under medium and heavy load conditions.

To verify theoretical analysis, three laboratory prototypes with 380–450 V input 120 V/10 A output based on CTR, FBR, and Hyb-R are built and tested, respectively. The measured efficiency shows the superiority of the proposed converter with Hyb-R over the converters with CTR and FBR.

## REFERENCES

- [1] B. Laska *et al.*, "Standardization of system architectures for onboard auxiliary power supply systems," in *Proc. 14th Int. Power Electron. Motion Control Conf.*, Sep. 2010, pp. S8-5–S8-9.
- [2] A. Kluge *et al.*, "Power electronics in railway lighting systems," in *Proc. IEEE Int. Conf. Ind. Technol.*, May 2010, pp. 793–799.
- [3] B. P. McGrath, D. G. Holmes, P. J. McGoldrick, and A. D. McIver, "Design of a soft-switched 6-kW battery charger for traction applications," *IEEE Trans. Power Electron.*, vol. 22, no. 4, pp. 1136–1144, Jul. 2007.
- [4] I. Quesada *et al.*, "Modulation technique for low frequency harmonic cancellation in auxiliary railway power supplies," *IEEE Trans. Ind. Electron.*, vol. 58, no. 9, pp. 3976–3982, Sep. 2011.

- [5] M. Helsper and M. A. Ocklenburg, "SiC MOSFET based auxiliary power supply for rail vehicles," in *Proc. 20th Eur. Conf. Power Electron. Appl.*, Sep. 2018, pp. 1–8.
- [6] C. Y. Inada, Y. Konishi, and M. Nakaoka, "High frequency transformer-assisted passive soft switching PWM DC-DC converter with energy recovery for compact auxiliary power supply in rolling stock transportation," in *Proc. 38th Annu. Meeting Ind. Appl. Conf.*, 2003, pp. 1906–1911.
- [7] A. A. Boora, F. Zare, A. Ghosh, and G. Ledwich, "Applications of power electronics in railway systems," in *Proc. Australas. Univ. Power Eng. Conf.*, 2007, pp. 1–9.
- [8] B. Whitaker *et al.*, "A high-density, high-efficiency, isolated on-board vehicle battery charger utilizing silicon carbide power devices," *IEEE Trans. Power Electron.*, vol. 29, no. 5, pp. 2606–2617, May 2014.
- [9] I. O. Lee, S. Y. Cho, and G. W. Moon, "Improved phase-shift PWM converter for larger sized PDP slim sustain power module," *IEEE Trans. Power Electron.*, vol. 28, no. 2, pp. 945–958, Feb. 2013.
- [10] D. Y. Kim, C. E. Kim, and G. W. Moon, "Variable delay time method in the phase-shifted full-bridge converter for reduced power consumption under light load conditions," *IEEE Trans. Power Electron.*, vol. 28, no. 11, pp. 5120–5127, Nov. 2013.
- [11] F. Musavi, M. Edington, W. Eberle, and W. Dunford, "A cost effective high-performance smart battery charger for off-road and neighborhood EVs," in *Proc. IEEE Transp. Electrific. Conf. Expo.*, Jun. 2012, pp. 1–6.
- [12] X. Ruan, *Soft-Switching PWM Full-Bridge Converters: Topologies Control and Design*. Hoboken, NJ, USA: Wiley, 2014.
- [13] V. R. K. Kanamarlapudi, B. Wang, N. K. Kandasamy, and P. L. So, "A new ZVS full-bridge DC-DC converter for battery charging with reduced losses over full-load range," *IEEE Trans. Ind. Appl.*, vol. 54, no. 1, pp. 571–579, Jan./Feb. 2018.
- [14] D. S. Wijeratne and G. Moschopoulos, "A ZVS-PWM full-bridge converter with reduced conduction losses," *IEEE Trans. Power Electron.*, vol. 29, no. 7, pp. 3501–3513, Jul. 2014.
- [15] A. Safaei, P. Jain, and A. Bakhshai, "A ZVS pulsewidth modulation full-bridge converter with a low-RMS-current resonant auxiliary circuit," *IEEE Trans. Power Electron.*, vol. 31, no. 6, pp. 4031–4047, Jun. 2016.
- [16] L. Zhao, H. Li, X. Wu, and J. Zhang, "An improved phase-shifted full-bridge converter with wide-range ZVS and reduced filter requirement," *IEEE Trans. Ind. Electron.*, vol. 65, no. 3, pp. 2167–2176, Mar. 2018.
- [17] X. Ruan and Y. Yan, "A novel zero-voltage and zero-current-switching PWM full-bridge converter using two diodes in series with the lagging leg," *IEEE Trans. Ind. Electron.*, vol. 48, no. 4, pp. 777–785, Aug. 2001.
- [18] B. Gu, J. S. Lai, N. Kees, and C. Zheng, "Hybrid-switching full-bridge DC-DC converter with minimal voltage stress of bridge rectifier, reduced circulating losses, and filter requirement for electric vehicle battery chargers," *IEEE Trans. Power Electron.*, vol. 28, no. 3, pp. 1132–1144, Mar. 2013.
- [19] J. Wang, B. Ji, H. Wang, N. Chen, and J. You, "An inherent zero-voltage and zero-current-switching full-bridge converter with no additional auxiliary circuits," *J. Power Electron.*, vol. 15, no. 3, pp. 610–620, May 2015.
- [20] H. Li, L. Zhao, C. Xu, and X. Zheng, "A dual half-bridge phase-shifted converter with wide ZVZCS switching range," *IEEE Trans. Power Electron.*, vol. 33, no. 4, pp. 2976–2985, Apr. 2018.
- [21] I. O. Lee and G. W. Moon, "Soft-switching DC/DC converter with a full ZVS range and reduced output filter for high-voltage applications," *IEEE Trans. Power Electron.*, vol. 28, no. 1, pp. 112–122, Jan. 2013.
- [22] I. O. Lee and G. W. Moon, "Analysis and design of phase-shifted dual H-bridge converter with a wide ZVS range and reduced output filter," *IEEE Trans. Ind. Electron.*, vol. 60, no. 10, pp. 4415–4426, Oct. 2013.
- [23] Z. Ye, "Dual half-bridge DC-DC converter with wide-range ZVS and zero circulating current," *IEEE Trans. Power Electron.*, vol. 28, no. 7, pp. 3276–3286, Jul. 2013.
- [24] W. Wang, H. Chen, X. K. Wu, and Z. Qian, "A novel hybrid half-bridge DC-DC converter with wide ZVS-range and high efficiency," in *Proc. IEEE Power Electron. Specialists Conf.*, 2004, pp. 511–515.
- [25] K. H. Park and K. H. Yi, "A wide load range ZVS dual half-bridge converters for large-sized PDP sustaining power modules," *J. Display Technol.*, vol. 11, no. 1, pp. 86–96, Jan. 2015.
- [26] I. D. Jitaru and N. D. Bolohan, "A high efficiency 2KW DC-DC converter for automotive application," in *Proc. 27th Annu. IEEE Appl. Power Electron. Conf. Expo.*, 2012, pp. 22–27.
- [27] R. Burkel and T. Schneider, "Characteristics and applications of fast recovery epitaxial diodes," IXYS Corporation, Milpitas, CA, USA, *Appl. Note IXAN0044*, 1999.
- [28] Z. Chen, S. Liu, L. Shi, and F. Ji, "Power loss and analysis and comparison of two full-bridge converters with auxiliary networks," *IET Power Electron.*, vol. 5, no. 9, pp. 1934–1943, Nov. 2012.
- [29] K. B. Park, C. E. Kim, G. W. Moon, and M. J. Youn, "Voltage oscillation reduction technique for phase-shift full-bridge converter," *IEEE Trans. Ind. Electron.*, vol. 54, no. 5, pp. 2779–2790, Oct. 2007.
- [30] Z. Chen, L. Shi, F. Ji, and S. Liu, "Mechanism and suppression countermeasure of voltage oscillation for full bridge converter," *IET Power Electron.*, vol. 5, no. 8, pp. 1535–1543, 2012.
- [31] SMC Diode Solutions, 12TQ150 datasheet, 2006. [Online]. Available: [http://www.smc-diodes.com/products\\_info.asp?id=9848](http://www.smc-diodes.com/products_info.asp?id=9848)
- [32] IXYS, DPG151400PM datasheet, 2013. [Online]. Available: <http://ixapps.ixys.com/DataSheet/DPG151400PM.pdf>



**Lei Zhao** (M'19) was born in Anhui, China, in 1988. He received the B.S., M.S., and Ph.D. degrees in electrical engineering from the Harbin Institute of Technology, Harbin, China, in 2011, 2013, and 2018, respectively.

He is currently an Associate Professor with the Department of Electronic and Information Engineering, College of Engineering, Shantou University, Shantou, China. His research interests include power conversion and control technology.



**Zejia Luo** was born in Guangdong, China, in 1995. He received the B.S. degree in electrical engineering from Wuyi University, Jiangmen, China, in 2018. He is currently working toward the M.S. degree in electrical engineering with Shantou University, Shantou, China.

His current research interests include power conversion and control technology.



**Zhun Fan** (SM'10) received the B.S. and M.S. degrees in control engineering from the Huazhong University of Science and Technology, Wuhan, China, in 1995 and 2000, respectively, and the Ph.D. degree in electrical and computer engineering from Michigan State University, Lansing, MI, USA, in 2004.

He is currently a Full Professor with Shantou University, Shantou, China. His major research interests include intelligent control and robotic systems, robot vision and cognition, MEMS, computational intelligence, design automation, optimization of mechatronic systems, machine learning, and image processing.



**Yi Shi** was born in Jiangxi, China, in 1990. He received the B.S. and Ph.D. degrees in instrument science and technology from Tianjin University, Tianjin, China, in 2012 and 2018, respectively.

He is currently an Assistant Professor with the Department of Electronic and Information Engineering, College of Engineering, Shantou University, Shantou, China. His research interests include optical fiber sensor, smart sensor, digital signal processing, and mode recognition.